IOPscience iopscience.iop.org

Home Search Collections Journals About Contact us My IOPscience

Effects of crystal orientation on electronic band structure and anomalous shift of higher critical point in VO_2 thin films during the phase transition process

This content has been downloaded from IOPscience. Please scroll down to see the full text.

2015 J. Phys. D: Appl. Phys. 48 485302

(http://iopscience.iop.org/0022-3727/48/48/485302)

View the table of contents for this issue, or go to the journal homepage for more

Download details:

IP Address: 222.204.247.68
This content was downloaded on 10/11/2015 at 07:05

Please note that terms and conditions apply.

IOP Publishing Journal of Physics D: Applied Physics

J. Phys. D: Appl. Phys. **48** (2015) 485302 (10pp) doi:10.1088/0022-3727/48/48/485302

Effects of crystal orientation on electronic band structure and anomalous shift of higher critical point in VO_2 thin films during the phase transition process

Peng Zhang[1], Ting Huang[1], Qinghu You[2], Jinzhong Zhang[1], Wenwu Li[1], Jiada Wu[2], Zhigao Hu[1] and Junhao Chu[1]

[1] Key Laboratory of Polar Materials and Devices, Ministry of Education, Department of Electronic Engineering, East China Normal University, Shanghai 200241, People's Republic of China
[2] Department of Optical Science and Engineering, Fudan University, Shanghai 200433, People's Republic of China

E-mail: zghu@ee.ecnu.edu.cn

Received 19 August 2015, revised 24 September 2015
Accepted for publication 6 October 2015
Published 5 November 2015

Abstract

The phase transition behaviour of vanadium dioxide (VO_2) with different thicknesses has been investigated by temperature-dependent optical transmittance and Raman spectra. It is found that the crystal orientation has a great effect on the metal-insulator transition (MIT) of VO_2 films. The x-ray diffraction (XRD) analysis shows that the films are polycrystalline and exhibit the characteristics of the monoclinic phase. The preferential growth crystal orientation (0 2 0) is converted to the ($\bar{1}$ 1 1) plane with the film thickness increasing. It is believed that the ($\bar{1}$ 1 1) plane is the reflection of a twinned structure with (0 1 1) crystal orientation, which will lead to the arrangements of oxygen atoms and vanadium atoms deviating from the pure monoclinic structure. It is found that the highest order transition (E_3) is highly susceptible to the crystal orientation, whereas the lowest order transition (E_1) is nearly unaffected by it. The E_3 exhibits an anomalous temperature dependence with an abrupt blue-shift ($\sim$0.5 eV) in the vicinity of the metal-insulator transition (MIT) for VO_2 film with a thickness of 84 nm. The findings show that the empty σ^* band can be driven close to the Fermi level when the (0 2 0) orientation is converted to the ($\bar{1}$ 1 1) orientation. Compared to the VO_2 films with thicknesses of 39 and 57 nm, the E_3 decreases by 0.8 eV and the E_2 increases by about 0.1 eV at the insulator state for the VO_2 film with a thickness of 84 nm. The abnormal electronic transition and the variation of energy band is likely caused by the lattice distortion and V–V dimerisation deviation from the monoclinic a_m axis.

Keywords: vanadium dioxide, metal-insulator transition, crystal orientation, electronic transition, energy band distortion

(Some figures may appear in colour only in the online journal)

1. Introduction

Vanadium dioxide (VO_2) undergoes a first-order metal-insulator transition (MIT) between two crystalline phases at about 340 K. The low-temperature phase is described by insulator behaviour with a monoclinic structure (M_1, $P2_1/c$). The high-temperature phase is metallic with a rutile structure (R, $P4_2/mnm$). This transition is accompanied by an abrupt change in resistivity by several orders of magnitude [1, 2]. The structural and electronic transition begins with two alternative starting points: a Peierls MIT driven by instabilities in electron-lattice dynamics and a Mott MIT, where strong

 © 2015 IOP Publishing Ltd Printed in the UK

electron–electron correlations drive charge localisation [3, 4]. Much effort has been made on the physical origin of the MIT due to potential applications in optics, sensing and high-density memories [5]. Involving both electronic and lattice degrees of freedom, several factors are known to affect the characteristics of MIT, such as doping [6, 7], strain [8, 9], oxygen vacancy [10, 11], grain size [12, 13] etc.

The dynamics of VO_2 thin films grown on different substrates and the associated phase transition modulation have become an important topic in recent years. It has been found that the crystal orientation of substrate has a great influence on the phase transition temperature. The MIT temperature (T_{MIT}) can be reduced to about 300 K for VO_2 thin film grown on (0 0 1) TiO_2, whereas the T_{MIT} was about 370 K for VO_2 film (∼10 nm) grown on (1 0 0) TiO_2 [14, 15]. The optical properties of VO_2 film deposited on sapphire with different orientations was discussed in the recent literature [16]. They believed that the terahertz transmission properties can be tuned by the substrate crystal orientation. Most of the reports pay attention to the effects of the substrate on the properties of VO_2 film, whereas the influence of the crystal orientation of VO_2 film deposited on the same substrate on the electronic transition and band structure is scarcely addressed.

In this study, VO_2 films with different thicknesses were grown on c-Al_2O_3 (0001) substrates. The XRD results show that the crystal orientation ($\bar{1}$ 1 1) presents the twinned crystal structure, which is the origin of the octahedra distortion in VO_2. The effect of the crystal orientation of VO_2 films on electronic transition is systematically studied. It is found that the highest order transition does not show the common hysteresis loop for VO_2 films with different thicknesses. Intriguingly, an abnormal hop has been observed in the vicinity of the MIT for VO_2 film with ($\bar{1}$ 1 1) plane. This phenomenon indicates that the energy band distortion can be induced by lattice disorder at the insulator state. According to the variation of electronic transition energy, the energy band shift diagram has been constructed to illustrate the impact of the crystal orientation.

2. Experimental details

The pulsed laser deposition (PLD) technique was used to grow VO_2 thin films on Al_2O_3 (0001) substrates. In order to obtain better crystalline quality, the substrates were rigorously cleaned in pure ethanol with an ultrasonic bath and were rinsed several times by deionised water before the deposition. The energy density of the laser beam at the target surface was maintained at 2 J $cm^{-2}$with a target-substrate distance of 6 cm. The VO_2 target was prepared from VO_2 powder (purity 99.95%). The vacuum chamber was evacuated down to 5×10^{-3} Pa. The oxygen partial pressure of the chamber was maintained at 20 mTorr during the deposition process. The deposition times were 30, 45 and 55 min, respectively. After deposition at room temperature (RT), amorphous films were annealed at 450 ℃ in nitrogen ambience by a thermal process for 1 h to obtain crystalline VO_2 films. The systematic study of growth conditions can also be found elsewhere [17].

The thicknesses of the VO_2 films are estimated to be about 39, 57 and 84 nm from measurement by scanning electron microscopy (SEM: Philips XL30FEG). The microstructure structures of the VO_2 films were studied by x-ray diffraction (XRD) with Cu $K\alpha$ radiation ($\lambda = 0.1542$ nm). To characterise the transport properties across the phase transition boundary, the resistance was measured by a THMSE 600 heating/cooling stage (Linkam Scientific Instruments) in the temperature range from 273 to 373 K. X-ray photoelectron spectroscopy (XPS, AXIS Ultra^{DLD}, Japan) with Al $K\alpha$ radiation ($h\nu = 1486.6$ eV) was performed to investigate the valence state and the stoichiometry of the films. The normal-incident transmittance spectra at the temperature range of 298–373 K were recorded using a double beam ultraviolet-infrared spectrophotometer (PerkinElmer Lambda 950) at the photon energy from 0.5 to 6.5 eV (190–2650 nm). The VO_2 films were mounted into a heating stage (Bruker A599) for the high-temperature experiment. Temperature-dependent Raman spectra were collected with a Jobin-Yvon LabRAM HR 800 micro-Raman spectrometer and a THMSE 600 heating/cooling stage (Linkam Scientific Instruments) in the temperature range from 290 to 373 K. A laser with a wavelength of 488 nm (2.54 eV) was applied as the exciting light.

3. Results and discussions

The XRD θ–2θ patterns of VO_2 films with different thicknesses are shown in figure 1(a). The diffraction peaks at $2\theta = 27.88°$ originate from the (0 1 1) plane of the monoclinic phase (M_1), which corresponds to the (1 1 0) plane of the rutile phase, and is known as preferential growth plane of polycrystalline VO_2 film [18]. It is found that the (0 1 1) peaks shift to a lower 2θ value as the films become thicker. The shift of the (0 1 1) peaks approaches about 0.1°. Note that the diffraction peak shift is subtle (0.02°) between the VO_2 films with thicknesses of 39 and 57 nm, whereas the shift reaches 0.08° between the VO_2 films with thicknesses of 39 and 84 nm. It is well known that the strain is the origin of the peak shift and the T_{MIT} can be reduced by strain [14, 19]. However, the T_{MIT} is about 345, 349 and 348 K for films with thicknesses of 39, 57 and 84 nm. This indicates that the three films are structurally relaxed and almost no strain remains in the films. For comparison, the transport behaviour of the VO_2 films grown on the (0 0 1) TiO_2 substrate is shown in figure 1(b). The T_{MIT} is about 303 and 313 K for the VO_2 films with thicknesses of about 10 and 25 nm, respectively. The results demonstrate that the T_{MIT} can be reduced to room temperature by strain, which is in good agreement with other reports [20, 21]. Therefore, the strain effect is insignificant and can be ignored from the above analysis in the present work. Then, the shift of the (0 1 1) peaks can be attributed to the crystal orientation transformation or the change of the internal octahedra structure.

It can be seen that the intensity of the diffraction peaks (0 1 1) gradually increases and the full width at half maximum (FWHM) decreases with the film thickness. The quantification results can be seen in table 1. The results indicate that the crystal quality is improved with the film thickness. Note that

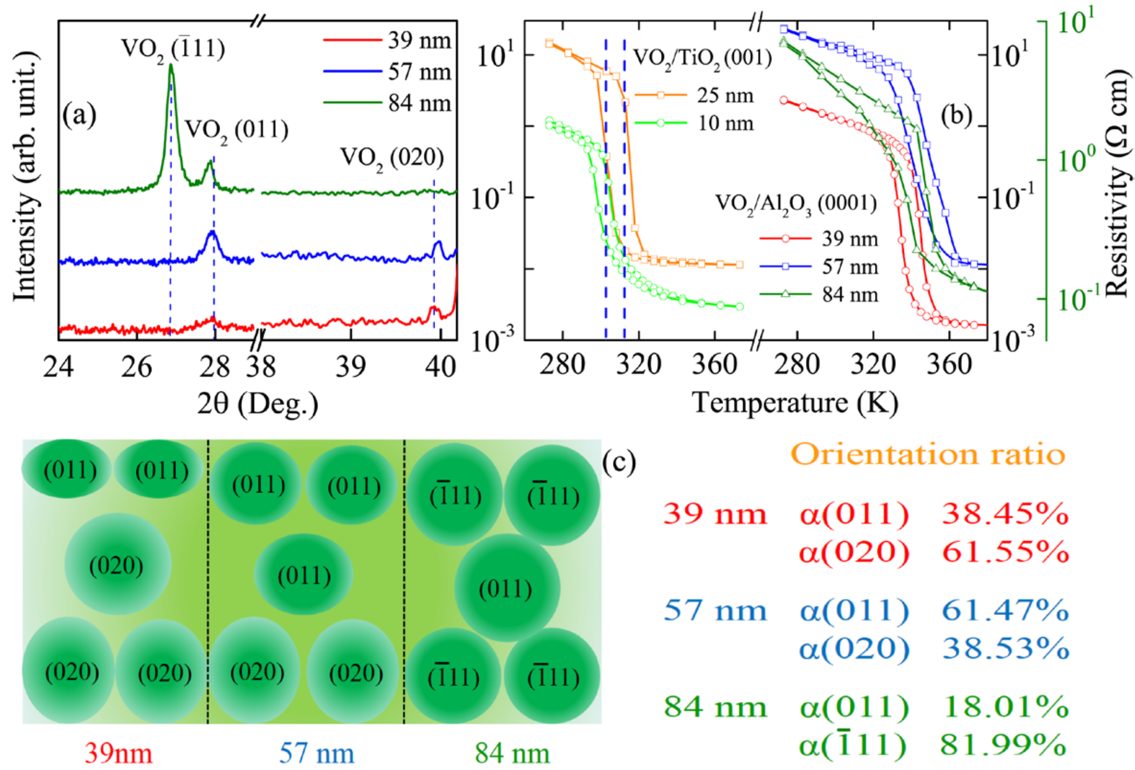

Figure 1. (a) The θ–2θ scan XRD curves for thickness-dependent VO_2 films. (b) The resistivity as the function of temperature for the VO_2 films with different thickness. The vertical coordinates with olive colour presents the resistivity of VO_2 film with a thickness of 84 nm to make the MIT process distinct. The degree of the orientation for VO_2 films with different thickness are shown in qualitative pattern of left figure (c). The right diagram is the ratios of the crystal orientation.

Table 1. The position and FWHM of the (−1 1 1) and (0 1 1) diffraction peaks for the VO_2 films determined from the XRD patterns in figure 1.

	Peak position/°			FWHM/°		d_{hkl}/Å		Grain size nm^{-1}	
Samples	(0 1 1)	(0 2 0)	($\bar{1}$ 1 1)	(0 1 1)	($\bar{1}$ 1 1)	(0 1 1)	($\bar{1}$ 1 1)	(0 1 1)	($\bar{1}$ 1 1)
39 (nm)	27.935	39.930	...	0.601	...	3.191	...	15.153	...
	(0.023)	(0.006)	...	(0.084)	...	(0.002)	...	(1.283)	...
57 (nm)	27.914	39.968	...	0.366	...	3.194	...	24.850	...
	(0.005)	(0.004)	...	(0.021)	...	(0.001)	...	(1.317)	...
84 (nm)	27.852	...	26.884	0.233	0.269	3.201	3.314	39.108	33.773
	(0.005)	...	(0.001)	(0.016)	(0.003)	(0.001)	(0.001)	(2.541)	(0.479)

Note: The 95% confidence limits are given in parentheses.

the the peaks at $2\theta = 39.93°$ are derived from the (0 2 0) plane for VO_2 film with thicknesses of 39 and 57 nm. However, the (0 2 0) peak is absent for the VO_2 film with a thickness of 84 nm instead of another peak at $2\theta = 26.87°$, which originates from the ($\bar{1}$ 1 1) plane of the M_1 phase. According to the nucleation phenomenon and crystal growth tendency, VO_2 prefers to texture along the low-energy plane of the monoclinic phase [22, 23]. The low-energy plane is (0 1 1) and (0 2 0) for VO_2 film with thicknesses of 39 and 57 nm. It is strange that the ($\bar{1}$ 1 1) plane occurs for the thickest VO_2 film, which is not the priority low-energy plane. It is well known that the VO_2 film grown on the (0001) Al_2O_3 substrate usually possesses (0 2 0) orientation even at rather thicker thicknesses, while presenting the (0 1 1) plane on the SiO_2 substrate by PLD. In this study, the (0 2 0) and (0 1 1) peaks can be found from the XRD results for the VO_2 film with thicknesses of 39 and 57 nm. However, it is strange that the (0 2 0) peak does not grow on the (0001) Al_2O_3 substrate for the thickest film. In the previous study, the preferred orientation of (0 1 1) disappeared and was split into ($\bar{2}$ 0 1) and (2 0 1) peaks, which is the signal of the twinned structure for the VO_2 film grown on the SiO_2 substrate [18, 24]. Similarly, it can be believed that the formation of the twinned structure may lead to the epitaxial relationship disappearing. According to the viewpoint of Nagashima *et al* the line cracks can be formed on the surface of epitaxial films, where the twinned structure can survive [25]. Balakrishnan *et al* reported that the twinned structure can be formed in proximal crack regions [26].

We inferred that there most likely exists a critical thickness, beyond which the role of the line cracks cannot be

ignored [25], and the cracks promote the formation of the twinned structure. Therefore, the splitting phenomenon can be observed at the VO_2 film with a thickness of 84 nm. Furthermore, it is believed that the strain relaxation on the interface of the line cracks tends to occur with increasing the film thickness and the lattice constant can be changed due to the thermal stress relaxation effects during the annealing process [27]. The formation of the twinned structure and the larger grain size may enhance the distortion of the monoclinic structure. Therefore, it can be believed that the epitaxial relationship may disappear and the vanishing of the (0 2 0) peak is the resultant action of the above force. It has been found that the ($\bar{2}$ 1 1) is the symbol of the formation of the twinned crystal structure with (2 0 0) crystal orientation for VO_2 film grown on the *r* cut Al_2O_3 substrate [16, 28]. They believed that the ($\bar{2}$ 1 1) and (2 0 0) orientation is derived from the (0 1 1) plane. It should be noted that the ($\bar{1}$ 1 1) orientation is nearly along the (0 1 1) orientation for the present thickest film. The result shows that the (0 1 1) orientation can be regarded as the origin of the ($\bar{1}$ 1 1) plane. It is inferred that the ($\bar{1}$ 1 1) and (0 1 1) orientations can result in the formation of a twinned crystal structure, which will lead to a higher energy plane and energy barrier. The calculation of grain size below verifies the speculation of the twinned crystal structure formation.

Transmission electron microscopy is a direct way to observe the twinned structure, and which was often used to observe microcrystals [26, 29]. It was found that twinned grains recorded at high magnification were formed near the crack, and the size of the grain is nearly same. Li *et al* also hinted that the information of the twinned grain can be obtained from comparison of the grain size [30]. Therefore, the grain size is calculated below through the present XRD results. However, the information of the twinned grain can also be picked up from the XRD results. It is reported that the periodical twinned structure of the M_2 phase can be identified from the XRD peaks. The (0 1 1) plane can be split into ($\bar{2}$ 0 1) and (2 0 1) peaks under different deposition conditions, such as different deposition power [18, 24]. In the present study, the ($\bar{1}$ 1 1) plane can be attributed to the M_1 phase. Li *et al* regarded that the diffraction spots of the $(\bar{1}\ \bar{1}\ 1)_M$ is related to the twinned structure, which originates from the $[1\ 0\ 1]_M$ zone axis [30]. Wong *et al* noted that the 011-type reflections splitting was not observed. while Chen *et al* and Zhao *et al* observed the peak splitting phenomenon in the 011-type reflection of ø scans, which is the signal of the formation of a twinned structure [16, 31, 32]. Combining the above analysis, it can be believed that the splitting of the (0 1 1) peak is the symbol of the twinned structure. In addition, the twinned grains can also be reflected by the grain size calculation.

It is strange that the transmittance of the VO_2 film with a twinned structure is relatively low at the insulator state and the transmittance drop is only 30% [30]. Generally, the transmittance of the VO_2 film with a thickness of 70 nm can approach 75% at the insulator state and the transmittance drop is at least 50% through temperature. This phenomenon is similar to the transmittance results of the VO_2 film with a thickness of 84 nm, which may be taken as a signal of the existence of the twinned structure. The transmittance results will be discussed in detail below. It is believed that the line cracks will be formed on the surface of epitaxial films, where the twinned structure can survive [25, 26]. The resistance in these line cracks is generally known to be very high and the present resistance results are in good agreement with that [33]. It should be noted that the line cracks cannot be found if the film is totally strained by the substrate. However, the strain relaxation will occur with increasing the film thickness. For example, the line cracks can be found on the surface of the VO_2/TiO_2 film with a thickness of 30 nm, while the line cracks are non-existent for the VO_2/TiO_2 film with a thickness of 10 nm. In this case, the twinned structure will be formed in the region where the strain is relaxed. Therefore, the twinned structure only confined to a small thickness on the surface of the film. In the present study, the film is almost totally relaxed. Then, it is inferred that the twinned structure likely exists in most regions of the films.

According to the well-known Scherrer equation, $d = k\lambda/\beta\cos\theta$, the average grain size r can be calculated to be about 15, 25 and 39 nm from the (0 1 1) diffraction peak for VO_2 film with thicknesses of 39, 57 and 84 nm, respectively. Where k, β, d, θ and λ is a constant, the FWHM, grain size, diffraction angle and wavelength of the x-ray, respectively. It should be noted that the (0 2 0) peak is beyond the application of the Scherrer equation and the (0 2 0) peak does not couple with the (0 1 1) plane. Therefore, the twinned structure cannot be formed by the (0 2 0) and (0 1 1) planes. It was found that the grain size (about 15 nm) of the VO_2 film with a thickness of 39 nm is the smallest, corresponding to the largest value of the full width at half maximum (FWHM). Furthermore, the grain size gradually increases with the VO_2 film thickness, which is consistent with a previous report [13]. The grain size is about 34 nm from the peak of ($\bar{1}$ 1 1), which is nearly the same as that from the calculation of the (0 1 1) peak for the thickest film. The similar grain size and the derivation ($\bar{1}$ 1 1) orientation along the (0 1 1) plane show that the twinned crystal is formed in the thickest film. It is well known that the formation of twinned crystal is to be expected if a structure phase transition takes place from a space group to another less symmetric space group [34]. Therefore, it is credible that the monoclinic structure is distorted along the rutile (1 1 0) during the formation of the twinned crystal.

For characterising the degree of the orientation with the film thickness, the magnitudes of the (0 1 1), (0 2 0) and ($\bar{1}$ 1 1) orientations (α(0 1 1), α(0 2 0)) and α($\bar{1}$ 1 1) are defined as the ratios of intensity of a peak to the sum of intensities of all peaks in the XRD patterns, and the formula can be written as: [35]

$$\alpha_{(0\,1\,1)} = \frac{I_{(0\,1\,1)}}{\sum_{\text{all peaks}} I_{(hkl)}}. \qquad (1)$$

$$\alpha_{(0\,2\,0)} = \frac{I_{(0\,2\,0)}}{\sum_{\text{all peaks}} I_{(hkl)}}. \qquad (2)$$

$$\alpha_{(\bar{1}\,1\,1)} = \frac{I_{(\bar{1}\,1\,1)}}{\sum_{\text{all peaks}} I_{(hkl)}}. \qquad (3)$$

where $I_{(0\,1\,1)}$, $I_{(0\,2\,0)}$, $I_{(\bar{1}\,1\,1)}$ and $\sum_{\text{all peaks}} I_{hkl}$ are the intensities of the peaks (0 1 1), (0 2 0), ($\bar{1}$ 1 1) and the sum of intensities of all peaks in the XRD patterns, respectively. The qualitative orientation picture and the ratio of the diffraction peaks are shown in figure 1(c). Note that the size of the circle presents the grain size except the (0 2 0) plane. From the picture, the ratio of the ($\bar{1}$ 1 1) reaches 82%, indicating the higher energy plane is dominant over the properties of VO_2 film with a thickness of 84 nm. It is believed that the ($\bar{1}$ 1 1) plane will lead to the oxygen atoms and vanadium atoms rearranging, which is similar to that in the (1 1 0) plane of tetragonal VO_2 [16, 28]. Considering the β mismatch for VO_2 film grown on *c* cut Al_2O_3 substrate, the octahedra in VO_2 can be orthorhombically distorted, making it possible to differentiate the apical and equatorial V–O bonds of the monoclinic structure [31]. However, the preferential crystal orientation plays a principal part for the VO_2 film with thicknesses of 39 and 57 nm, which indicates that the initial state is a pure monoclinic structure.

Figure 1(b) summarises the transport behaviour of VO_2 films with different thicknesses. It can be seen that the T_{MIT} is 344.7, 348.8 and 348.4 K for the VO_2 film with thicknesses of 39, 57 and 84 nm through the derivative of resistivity against temperature, respectively. It should be noted that the difference of the T_{MIT} is about 4 K for the VO_2 film with thicknesses of 39 and 57 nm, and the T_{MIT} is nearly the same for the VO_2 film with thicknesses of 57 and 84 nm. Generally, the difference of thermal the expansion coefficient between VO_2 and Al_2O_3 results in rather high T_{MIT} for VO_2-on-Al_2O_3 when VO_2 has the (0 2 0) orientation based on the anisotropic thermal coefficient of VO_2. In this study, it can be found that the difference of the T_{MIT} is inconspicuous and the resistivity drop is nearly the same for the VO_2 film with thicknesses of 39 and 57 nm. It can be concluded that the thermal expansion coefficient is not the main factor in the present study and the effect of the thermal expansion coefficient can be ignored. In order to highlight the MIT process of the thickest film, the olive vertical coordinates were used to present the variation of the resistivity. It is found that the resistivity drop approaches three orders of magnitude for the VO_2 films with thicknesses of 39 and 57 nm, while the resistivity drop is more than one order of magnitude for the thickest film. The MIT process of the thickest film is seemingly sharper than the other films during the heating process. It is strange that the cooling process shows a sluggish change for the thickest film. It has been reported that the intermediate state can lead to a resistivity drop of less than $\sim 10^3$ [36]. Kumar *et al* regarded that the asymmetry of the transport behaviour is a reflection of the monoclinic-metal phase and the rutile-insulator phase for the VO_2 film grown on Si_3N_4/Si substrate. Combining the above XRD analysis, it can be believed that the ($\bar{1}$ 1 1) orientation means the lattice distortion, which makes the V–V dimerisation deviate from the monoclinic a_m axis. This similar asymmetry phenomenon can also be seen from the optical characters below. Note that the resistivity increases with the film thickness at the metal state, which can be attributed to the occurrence of line cracks [25].

Figure 2(a) displays the overall core level XPS survey spectra of the VO_2 films with different thicknesses. Figures 2(b)–(g) shows the Lorentzian-Gaussian dividing peak analysis of V 2p and O 1s peaks after subtracting the Shirly background for the three films. The 1/2 and 3/2 spin–orbit doublet components of the V 2p photoelectron are found to be located at about 523.8 and 516.0 eV, respectively [37]. The peaks located at about 516.4, 515.7 and 516.0 eV for the three films are assigned to V^{4+}. This is consistent with the XPS analysis reported previously [37]. From the V 2p peaks, we cannot distinguish the existence of V^{5+} or V^{3+}. From the previous literature, V^{5+} or V^{3+} can be distinguished by the shoulder peak [38–40]. However, the shoulder peak of V^{5+} or V^{3+} cannot be observed in the present XPS spectra, indicating that the content of the V^{5+} or V^{3+} is subtle and can be ignored. On the contrary, the shoulder peak of the surface adsorption oxygen or hydroxyl contributions can be clearly observed from the O 1s spectra. The main peak located at about 530 eV can be assigned to O 1s. The shoulder peak located at about 532 eV should be attributed to the surface adsorption oxygen. Therefore, the effect of surface adsorption oxygen should be excluded while calculating the V: O ratios. The ratios of oxygen to vanadium are $VO_{2.042}$, $VO_{2.038}$ and $VO_{2.160}$ through a quantitative analysis of the XPS results. The effect of the stoichiometry of vanadium and oxygen will be discussed below.

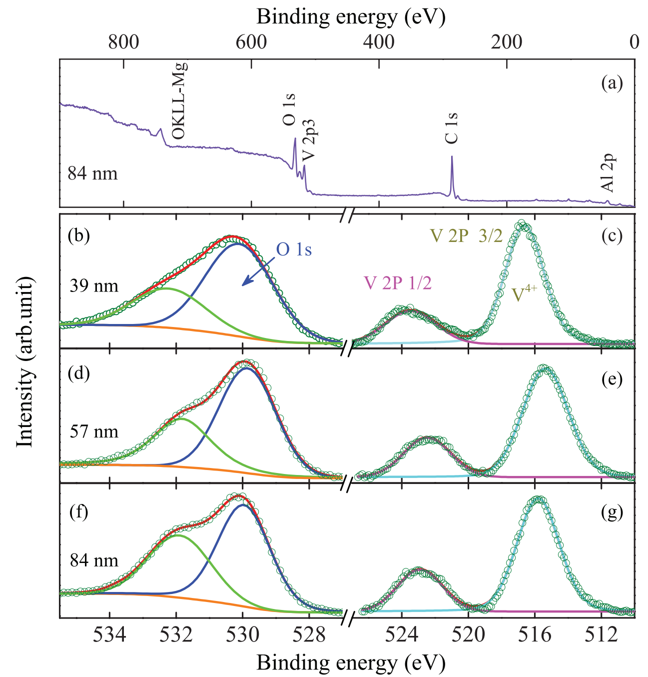

Figure 2. (a) Overall core level XPS spectra for VO_2 film with thickness of 84 nm. (b)–(g) is XPS spectra of V 2p lines and O 1s lines with the Lorentzian-Gaussian dividing peak analysis for the three films. The measured spectra are shown as olive circles and the reproduced curves are shown as solid lines.

In order to analyse the role of the compositional homogeneity on the MIT properties, the present results have been compared to the previous work done by Yang *et al* [41]. It is believed that the off-stoichiometric composition near the VO_2/SiO_2 interface induced by unoriented growth on amorphous SiO_2 is likely responsible for the dramatic change in transition characteristics. However, the VO_2 thin film on sapphire shows

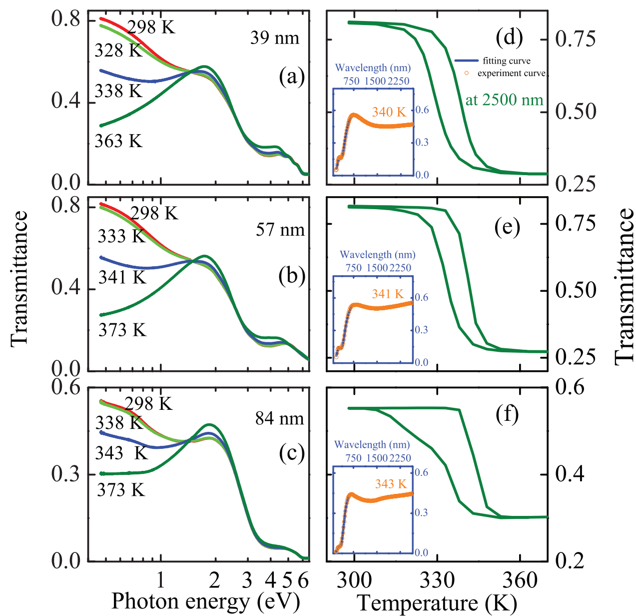

Figure 3. The transmittance spectra for VO_2 films are shown in (a)–(c). Note that the horizontal coordinate of photon energy is the logarithmic unit to enlarge the transparent region. The inset is the experimental (dotted lines) and best-fitted (solid lines) transmittance spectra of VO_2 films and the temperature dependence of infrared (IR) transmittance at selected incident photon energies are shown in (d)–(f).

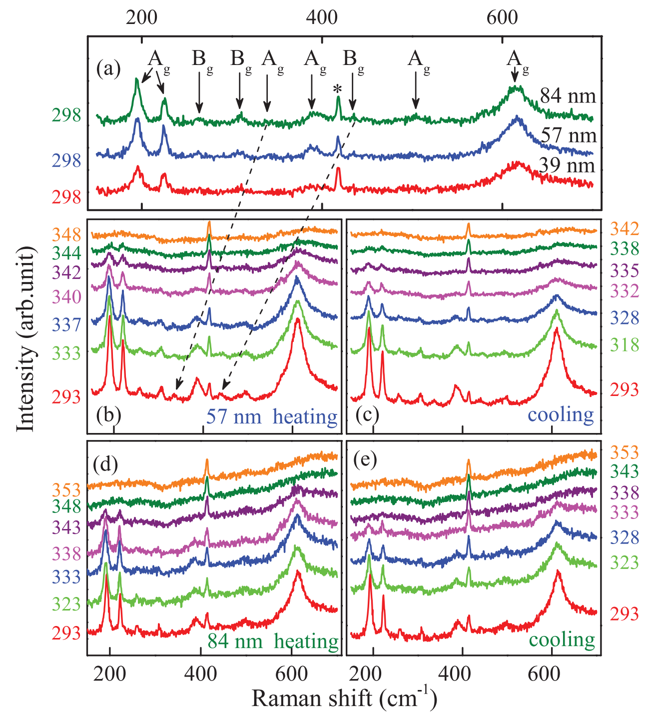

Figure 4. (a) Raman spectra at room temperatures for the VO_2 films with thickness of 39, 57 and 84 nm. (b) and (c) Raman spectra at different temperatures for the VO_2 film with thickness of 57 nm in the heating and cooling processes, respectively. (d) and (e) Raman spectra at different temperatures for the VO_2 film with thickness of 84 nm in the heating and cooling processes, respectively.

quite uniform phase transition characteristics across the film thickness. It is understandable that off-stoichiometric inhomogeneity is more easily induced by unoriented growth on amorphous SiO_2 than the oriented growth on a single crystal sapphire substrate. This indicates that the film tends to keep its homogeneity for the VO_2-on-sapphire, and the MIT properties changes little within the allowed stoichiometry. It is found that the peak assignment of V^{4+} and O1s in the present work is consistent with the XPS results measured by Yang *et al*. In addition, the stoichiometry is $VO_{2.042}$, $VO_{2.038}$ and $VO_{2.160}$ for the VO_2 films with thicknesses of 39, 57 and 84 nm, which is within the variation of the ratios of oxygen to vanadium reported by the group of Ramanathan [41]. If the sharp resistivity drop is caused by the compositional homogeneity in the present study, the T_{MIT} should differ greatly. However, the T_{MIT} is nearly the same for the VO_2 films with thicknesses of 57 and 84 nm, which can be reflected by the derivation of the resistivity. It is believed that the decreased resistivity drop can be induced by line cracks and the twinned crystal can be formed around the cracks [25, 26]. Therefore, it can be believed that the compositional homogeneity does not play a crucial role in the variation of the MIT properties.

The temperature-dependent normal-incident transmittance spectra are shown in figures 3(a)–(c). The three films display significant changes in the infrared range during the MIT process. From the temperature dependence of infrared (IR) transmittance at selected incident photon energies ($h\nu = 0.468$ eV, $\lambda = 2650$ nm), the transmittance variation at the infrared region is more than 50% for the VO_2 films with thicknesses of 39 and 57 nm, and is about 30% for the thickest film. It is found that the transmittance discrepancy is obvious between the thickest film and the other two films at the insulator state. However, the transmittance is nearly the same at the metal state for the three films. It has been generally agreed upon that the mechanism of the MIT in VO_2 is considered to be a collaborative Mott–Peierls transition, i.e. electronic-structure transition [42, 43]. Due to the $(\bar{1}\ 1\ 1)$ crystal orientation representing the crystal distortion and V–V dimerisation deviation, the transmittance spectra discrepancy can be attributed to the response of the lattice deviation. In addition, the MIT process is sharp for the thickest VO_2 film than the other two VO_2 films at the heating process from the loop of the IR transmittance. However, the cooling process shows a sluggish change for the VO_2 film with a thickness of 84 nm, which is similar to the transport behaviour of the film. The results further demonstrate that the monoclinic structure is distorted during the formation of the twinned crystal structure.

Figure 4(a) shows room temperature (298 K) Raman spectra (298 K) for the three VO_2 films, where the phonon modes can be uniquely assigned [44–46]. The distinct peaks located at about 194, 221 and 615 cm^{-1} demonstrate the three VO_2 films are of M_1 phase at room temperature, indicating the well crystalline structure. Comparing the vibrations at about 196 and 617 cm^{-1} for the VO_2 film with thicknesses of 39 and 57 nm, the characteristic peaks are located at about 194 and 614 cm^{-1} for the thickest film. The red shift of the vibrations can be attributable to the variation of the V chains and V–O vibration. Note that the peak located at about 414 cm^{-1} with

Table 2. Parameters of the Drude–Lorentz (DL) model for the VO_2 films extracted from the best fitting transmittance spectra at several temperatures.

Samples	39 nm			57 nm			84 nm		
T (K)	298	341	363	298	341	363	298	343	363
A_1	1.62 (0.01)	3.56 (0.01)	5.62 (0.34)	1.10 (0.01)	2.19 (0.10)	4.52 (0.21)	2.06 (0.03)	1.65 (0.31)	2.24 (0.51)
B_1 (eV)	1.01 (0.01)	0.95 (0.01)	0.94 (0.01)	0.98 (0.01)	1.24 (0.01)	0.82 (0.01)	2.77 (0.15)	1.43 (0.06)	1.05 (0.04)
E_1 (eV)	1.22 (0.01)	0.81 (0.01)	0.62 (0.02)	1.23 (0.01)	0.86 (0.01)	0.63 (0.02)	1.20 (0.02)	1.06 (0.01)	0.86 (0.02)
A_2	4.28 (0.03)	3.18 (0.05)	2.87 (0.05)	2.76 (0.02)	2.44 (0.06)	2.08 (0.07)	2.17 (0.21)	2.16 (0.05)	2.05 (0.06)
B_2 (eV)	1.98 (0.03)	1.53 (0.03)	1.40 (0.04)	2.40 (0.04)	1.79 (0.05)	1.43 (0.05)	1.26 (0.13)	1.71 (0.04)	1.64 (0.04)
E_2 (eV)	3.37 (0.01)	3.19 (0.01)	3.09 (0.01)	3.35 (0.01)	3.21 (0.01)	3.04 (0.13)	3.45 (0.04)	3.50 (0.01)	3.43 (0.01)
A_3	2.40 (0.08)	2.10 (0.04)	2.11 (0.04)	1.03 (0.06)	1.19 (0.03)	1.24 (0.03)	1.43 (0.16)	1.38 (0.05)	1.39 (0.04)
B_3 (eV)	3.07 (0.26)	3.50 (0.27)	3.63 (0.28)	2.60 (0.30)	4.36 (0.54)	4.15 (0.51)	2.50 (0.50)	3.20 (0.37)	2.86 (0.33)
E_3 (eV)	6.06 (0.09)	5.72 (0.06)	5.68 (0.08)	6.17 (0.13)	5.87 (0.12)	5.66 (0.11)	5.37 (0.16)	5.79 (0.08)	5.55 (0.06)
A_D	...	3.19 (0.43)	6.46 (0.08)	...	1.14 (0.29)	4.91 (0.09)	...	2.11 (0.55)	3.12 (0.46)
B_D (eV)	...	0.45 (0.10)	0.10 (0.01)	...	0.69 (0.10)	0.11 (0.01)	...	0.89 (0.27)	0.56 (0.14)

Note: The 90% confidence limits are given in parentheses.

the asterisk is the sign of the (0001) Al_2O_3 substrate. It is well known that the vibration modes of VO_2 are drastically different in the M_1 and R phase, the Raman scattering technique allows us to independently monitor the electronic and structural transitions. The structures of VO_2 are based on an oxygen (O) bcc lattice with vanadium (V) in the octahedral sites, and the O octahedra are more or less regular. The space groups for the monoclinic and rutile lattices are C_{2h}^3 and D_{4h}^{14}, respectively [47]. The monoclinic phase is thus characterised by 18 Raman-active phonons, while it has 4 Raman-active phonons in the R phase which exhibit strong polarisation dependence.

Figures 4(b)–(e) show the the lattice vibrations of the VO_2 film with thicknesses of 57 nm and 84 nm, respectively. Considering the electrical and optical properties are nearly same for the VO_2 film with thicknesses of 39 and 57 nm, we only give the temperature-dependent Raman spectral of VO_2 film with 57 nm as a comparison to that for the thickest film. The intense monoclinic A_g peaks can be observed at about 194, 220, 336, 386, 496 and 615 cm^{-1}, which is in accordance with the phonon frequencies reported by the previous Raman experiments [10, 47, 48]. In addition, the weaker peaks located at near 258, 307 and 440 cm^{-1} could be attributed to the B_g phonon modes. The low-frequency A_g phonon modes at 192 and 220 cm^{-1} can be assigned to the motion of V-ions in the dimerised chains due to the large difference between the V and O masses. The most pronounced high-frequency phonon modes at about 615 cm^{-1} are a feature of the V–O vibration [49]. These characteristic vibration modes of the M_1 phase are softened and eventually disappear as the temperature increases due to the high-temperature R phase. Conversely, these vibration modes emerge when the temperature is ramped down to a sufficiently low temperature. The Raman results demonstrate that the VO_2 films present the representative features of the monoclinic phase and the intensity characteristic peaks show the present VO_2 films are in a good crystalline structure.

In order to observe the effect of the structure deviation on the internal transition mechanism of the VO_2 film, the Drude–Lorentz (DL) oscillator dispersion relation is used to simulate the transmittance spectra, as in the following

$$\varepsilon(E) = \varepsilon_\infty - \frac{A_D}{E^2 + iEB_D} + \sum_{k=1}^{3} \frac{A_k}{E_k^2 - E^2 - iEB_k}. \quad (4)$$

Where ε_∞ is the high-frequency dielectric constant. A_k, E_k, B_k and E are the amplitude, centre energy, the broadening of the *j*th oscillator and the incident photon energy, respectively. The parameter A_D is the square of the plasma frequency and B_D is the electron collision or damping frequency. The inset is the best-fitted transmittance spectra of VO_2 films on sapphire substrates in figures 3(d)–(f). A good agreement can be observed, indicating that the dispersion model selected is reasonable. The parameter values of the three VO_2 films determined from the simulation of the transmittance spectra are shown in table 2. Note that the 90% confidence limits are given in the parameters.

The E_1 feature can be assigned to the transition from the lower V 3d filled $d_{//}$ band to the crystal field split 3d empty π^* band across the optical gap at other points in the Brillouin zone (BZ) [50]. Figure 5(a) shows the hysteresis loop of the centre energies of E_1. The E_1 energy is 1.22, 1.23 and 1.20 eV for the VO_2 films with thicknesses of 39, 57 and 84 nm, respectively. It is found that the E_1 is nearly the same at the insulator state with the film thickness, which indicates that the low-energy transition is nearly unaffected by the change in the crystal orientation or the structure deviation. It was reported that the band gap between the bottom of the empty π^* band and the top of the filled $d_{//}$ band is nearly unchanged under the effect of strain [19, 20]. One can see that the E_1, E_2 and E_3 is the transition from the centre of the conduction band to the centre of the valence band. In this study, we found that the low-energy transition of E_1 is nearly unaffected by the crystal orientation because the change in the transition energy is directly related to the variation of the band gap. In addition, it is found that the centre transition energy of E_1 presents the common hysteresis behaviour for the three VO_2 films. These results indicate that the low-energy transition is an inherent property of the VO_2 film, which does not suffer from the external or internal factors at the insulator state, such as crystal orientation or strain.

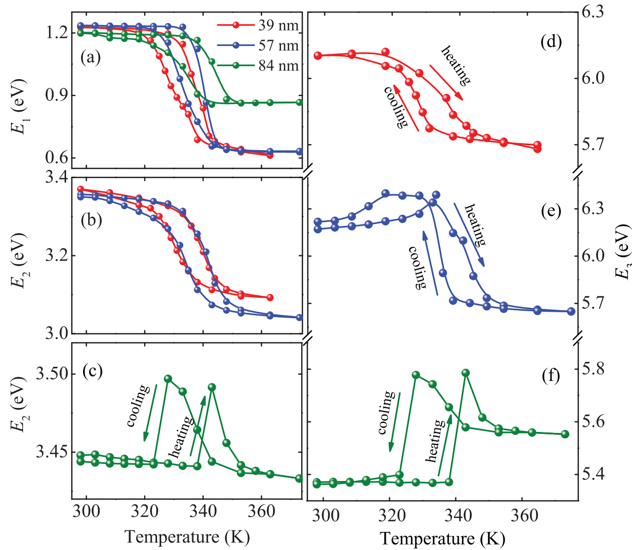

Figure 5. (a) The temperature dependent electronic transition of E_1 for the VO_2 films with thickness of 39, 57 and 84 nm, respectively. (b) and (c) is the transition energy of E_2 for the three films. The transition energy of E_3 for the three films was shown in (d)–(f).

The evolution of the centre transition energy of E_2 is shown in figures 5(b) and (c). The E_2 critical point can be interpreted to the transition between the filled O $2p$ π band to the empty π^* band [51]. The transition energy is 3.37, 3.35 and 3.45 eV with increasing film thickness at the insulator state. Compared to the VO_2 films with thicknesses of 39 and 57 nm, the transition energy increases by about 0.1 eV for the thickest film. Therefore, it can be concluded that the effect of the crystal orientation or the structure deviation is enhanced on the second-order transition at the insulator state. In the previous report [17], the E_2 transition energy is 3.40, 3.40 and 3.37 eV at the insulator state and the ratios of oxygen to vanadium is $VO_{1.895}$, $VO_{1.963}$ and $VO_{2.042}$, for the films grown at 5 mTorr, 10 mTorr and 20 mTorr, respectively. The variation of the transition energy at the insulator state is only 0.03 eV, much less than the 0.1 eV. Therefore, it can be concluded that the effect of the stoichiometry of vanadium and oxygen on the electronic transition is subtle and can be ignored at the insulator state. In addition, it should be noted that the E_2 is nearly same at the insulator state for the VO_2 film with thicknesses of 39 and 57 nm. Because the structural variation in VO_2 is accompanied by changes in the electronic band structure, the energy band structure will be distorted simultaneously during the lattice distortion and V–V dimerisation deviation.

It is observed that the E_2 transition follows a normal hysteresis behaviour for the VO_2 films with thicknesses of 39 and 57 nm. However, the E_2 energy shows an unusual relationship with the temperature for the thickest VO_2 film. There is a slight hop in the vicinity of the MIT. Note that the specific phenomenon has not been observed before. It is clear that the MIT process contains the structural variation as well as the electronic band change. Thus, the energy band near the Fermi surface is closely associated with the lattice structure and the vanadium–vanadium chain [52, 53]. For the VO_2 film with thicknesses of 39 and 57 nm, the initial structure is the common symmetry monoclinic structure and it will be turned into a rutile structure naturally during the MIT process. However, the distortion monoclinic structure is most likely rebounded to the symmetry monoclinic phase first because of the higher binding energy and energy plane for the VO_2 film with a thickness of 84 nm. Then it will be transformed into the rutile structure. Therefore, there is a slight hop during the MIT process. Furthermore, the spectral weight from the π^* and σ^* is most likely redistributed when the MIT occurs [54]. Koethe *et al* observed a giant transfer of spectral weight with distinct features across the MIT [55]. They stated that Auger emission may be responsible for this effect. Electrons on a conduction band can acquire extra energy from the electron-hole recombination process and be stimulated to a higher energy level. Therefore, the slight hop in the vicinity of the MIT may be caused by the combination mechanisms of the variation of the lattice structure, the energy transfer and the redistribution of the spectral weight.

Figures 5(d)–(f) show the temperature dependence of centre transition energy E_3. The transition can be assigned to the excitation from a lower V 3d filled $d_{//}$ band to an empty σ^* band [56]. At the insulator state, the transition energy is 6.06, 6.17 and 5.37 eV with the film thickness, respectively. It is found that the variation of the transition energy (ΔE_3) is distinguishable (~0.8 eV) between the VO_2 film with thicknesses of 39 and 84 nm. It can be concluded that the high energy band (σ^*) was more easily distorted by the transmutative monoclinic structure than the $d_{//}$, π and π^* band. Note that the transition energy increases slowly with the temperature at the insulator state and does not follow the Bose–Einstein relationship. The abnormal phenomenon was also reported by Li *et al* [57]. It was believed that the strong V_d–O_p hybridisation and V–V interaction can be obviously changed with temperature, which may not follow the Bose-Einstein formula. It will drive the σ^* band correspondingly shifting with the temperature. In addition, the higher electronic transition would result in a higher electronic density of states in O_{2p} states [39]. Therefore, the above mechanisms can contribute to the abnormal variation. It is worth noting that there is a serious hop (~0.5 eV) in the vicinity of the MIT for the film with a thickness of 84 nm. The serious hop shows that the higher energy transition is more sensitive to the lattice distortion and the redistribution of the σ^* band. Because the σ^* band is in a high energy state, it easily suffers from the variation of the lattice structure than the lower energy state of $d_{//}$, π and π^*. It was reported that the variation of gap (not fundamental gap) between the π band to the empty π^* band reached 0.7 eV in Mg-doped VO_2 films [58]. Therefore, it can be concluded that the higher electronic transition is highly susceptible to external or internal force.

From the above analysis, a clear picture of the electronic band diagram can be constructed, as shown in figure 6. It has been reported that the energy band distortion phenomenon can be induced by the substrate strain for VO_2 film grown on (0 0 1) TiO_2 substrate [19, 20]. The degree of the energy band distortion gradually changes with strain. In addition, the position of the antibonding band and the bonding band will be changed together under the role of the strain. In the present study, the strain is relaxed for the VO_2 film grown on a (0001) Al_2O_3 substrate. However, the energy shift phenomenon still exists.

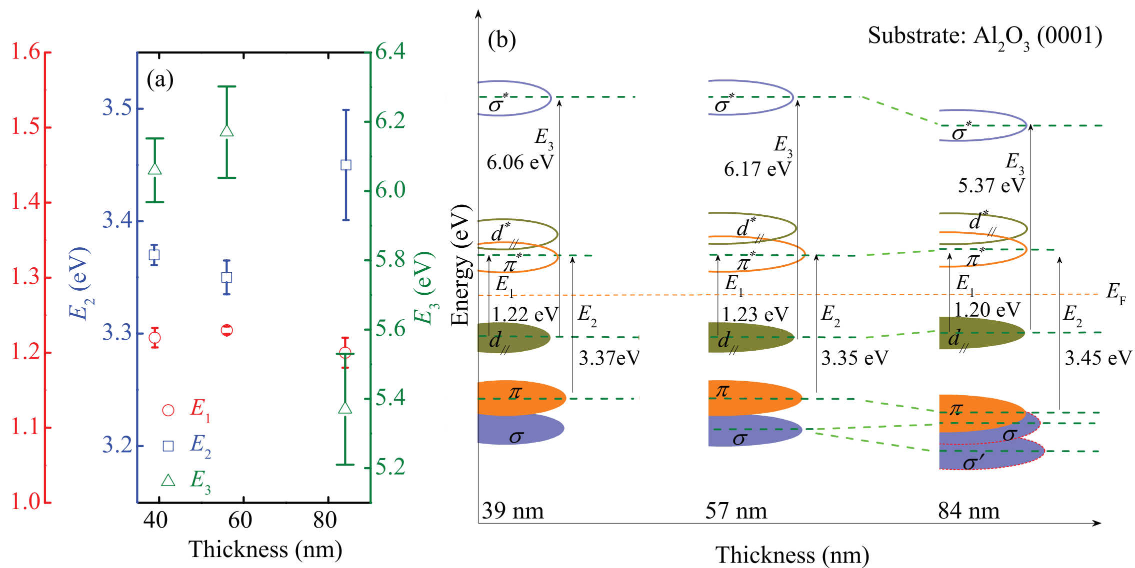

Figure 6. (a) The variation of the transition energy of E_1, E_2 and E_3 at insulator state as a function of film thickness. (b) The band scheme for VO_2 films at the insulator states with the film thickness. Note that the uncertainty is shown by σ and σ' in the band diagram.

Therefore, it is plausible that the similar energy band distortion can be induced by the crystal orientation. Furthermore, it is found that the condition of the energy band is nearly the same for the VO_2 film with thicknesses of 39 and 57 nm. The result also illustrates that the transformation of crystal orientation can induce the energy band change. From the transition energy, the shift of the $d_{//}$, π, π^* and σ^* band is observed in the present work. It is found that the E_3 energy decreases by about 0.8 eV for the VO_2 film with a thickness of 84 nm. Therefore, a lower V 3d filled $d_{//}$ band and the empty σ^* shift to E_F simultaneously. E_1 is the transition from the filled $d_{//}$ band to the empty π^* band, which is nearly unaffected by the transmutative monoclinic structure. Therefore, the empty π^* band will keep away from the E_F while the $d_{//}$ band is close to that. The filled π band will shift away from E_F, which can be reflected by the larger E_2 energy in the thickest film. It is certain that the empty σ^* shifts to E_F according to the E_3 energy, whereas the condition of the filled σ band is vague. This is because there is no transition directly related to the filled σ band in the present study.

4. Conclusions

In conclusion, the effects of crystal orientation on electronic transitions have been studied by temperature-dependent optical transmittance. The XRD results reveal that the twin crystal structure can be induced by the high-energy $(\bar{1}\ 1\ 1)$ plane. The temperature-dependent Raman results indicate that the VO_2 films display the representative characteristics of the monoclinic phase, confirming that the present VO_2 films are in good crystalline structure. The VO_2 film with a thickness of 84 nm shows an abnormal higher electronic transition in the vicinity of MIT. This can be attributed to the redistribution of the filled π band, the empty π^* band and the empty σ^* band as well as the crystal structure transformation. It is claimed that the energy band structure can be distorted by the structural deviation. It is found that the empty σ^* band is more sensitive to the variation of the crystal structure. The results may be helpful to identify the relationship between the distortion of energy band structure and the variation of crystal orientation.

Acknowledgment

This work was financially supported by the Major State Basic Research Development Program of China (Grant Nos. 2011CB922200 and 2013CB922300), the Natural Science Foundation of China (Grant Nos. 11374097 and 61376129), Projects of Science and Technology Commission of Shanghai Municipality (Grant Nos. 15JC1401600, 14XD1401500, 13JC1402100, and 13JC1404200), and the Program for Professor of Special Appointment (Eastern Scholar) at Shanghai Institutions of Higher Learning.

References

[1] Morin F J 1959 *Phys. Rev. Lett.* **3** 34
[2] Morrison V R, Chatelain R P, Tiwari K L, Hendaoui A, Bruhacs A, Chaker M and Siwick B J 2014 *Science* **346** 445
[3] Budai J D *et al* 2014 *Nature* **515** 535
[4] Rice T M, Launojs H and Pouget J P 1994 *Phys. Rev. Lett.* **73** 3042
[5] Nakano M, Shibuya K, Okuyama D, Hatano T, Ono S, Kawasaki M, Iwasa Y and Tokura Y 2012 *Nature* **487** 459
[6] Takami H, Kanki T, Ueda S, Kobayashi K and Tanaka H 2012 *Phys. Rev.* B **85** 205111
[7] Chen S, Liu J J, Wang L H, Luo H J and Gao Y F 2014 *J. Phys. Chem.* C **118** 18938
[8] Liu W T, Cao J, Fan W, Hao Z, Martin M C, Shen Y R, Wu J and Wang F 2011 *Nano Lett.* **11** 466
[9] Shibuya K, Tsutsumi J, Hasegawa T and Sawa A 2013 *Appl. Phys. Lett.* **103** 021604
[10] Zhang S X, Kim I S and Lauhon L J 2011 *Nano Lett.* **11** 1443
[11] Fan L L, Chen S, Wu Y F, Chen F H, Chu W S, Chen X, Zou C W and Wu Z Y 2013 *Appl. Phys. Lett.* **103** 131914

[12] Brassard D, Fourmaux S, Jean-Jacques M, Kieffer J C and El Khakani M A 2005 *Appl. Phys. Lett.* **87** 051910
[13] Lopez R, Haynes T E and Boatner L A 2002 *Phys. Rev.* B **65** 224113
[14] Kittiwatanakul S, Wolf S A and Lu J W 2014 *Appl. Phys. Lett.* **105** 073112
[15] Muraoka Y and Hiroi Z 2002 *Appl. Phys. Lett.* **80** 583
[16] Zhao Y, Lee J H, Zhu Y H, Nazari M, Chen C H, Wang H Y, Bernussi A, Holtz M and Fan Z Y 2012 *J. Appl. Phys.* **111** 053533
[17] Zhang P, Jiang K, Deng Q L, You Q H, Zhang J Z, Wu J D, Hu Z G and Chu J H 2015 *J. Mater. Chem.* C **3** 5033
[18] Okimura K, Watanabe T and Sakai J 2012 *J. Appl. Phys.* **111** 073514
[19] Fan L L *et al* 2014 *Nano Lett.* **14** 4036
[20] Nagaphani B A *et al* 2013 *Nat. Phys.* **9** 661
[21] Yajima T, Ninomiya Y, Nishimura T and Toriumi A 2015 *Phys. Rev.* B **91** 205102
[22] Sohn J I, Joo H J, Porter A E, Choi C J, Kim K, Kang D J and Welland M E 2007 *Nano Lett.* **7** 1570
[23] Frenzel A, Qazilbash M M, Brehm M, Chae B G, Kim B J, Kim H T, Balatsky A V, Keilmann F and Basov D N 2009 *Phys. Rev.* B **80** 115115
[24] Sohn J I, Joo H J, Ahn D, Lee H H, Porter A E, Kim K, Kang D J and Welland M E 2009 *Nano Lett.* **9** 3392
[25] Nagashima K, Yanagida T, Tanaka H and Kawai T 2006 *Phys. Rev.* B **74** 172106
[26] Balakrishnan V, Ko C and Ramanathan S 2012 *J. Mater. Res.* **27** 1476
[27] Thouless M D 1990 *J. Am. Ceram. Soc.* **73** 2144
[28] Yang T H, Aggarwal R, Gupta A, Zhou H, Narayan R J and Narayan J 2010 *J. Appl. Phys.* **107** 053514
[29] Yang T H, Jin C M, Zhou H H, Narayan R J and Narayan J 2010 *Appl. Phys. Lett.* **97** 072101
[30] Li X, Gloter A, Gu H, Cao X, Jin P and Colliex C 2013 *Acta Mater.* **61** 6443
[31] Chen C, Zhu Y, Zhao Y, Lee J H, Wang H, Bernussi A, Holtz M and Fan Z Y 2010 *Appl. Phys. Lett.* **97** 211905
[32] Wong F J, Zhou Y and Ramanathan S 2013 *J. Cryst. Growth* **364** 74
[33] Copetti C A, Schubert J, Zander W, Soltner H, Poppe U and Buchal C 1993 *J. Appl. Phys.* **73** 1339
[34] Fillingham P J 1967 *J. Appl. Phys.* **38** 4823
[35] Zhang J Z, Chen X G, Jiang K, Shen Y D, Li Y W, Hu Z G and Chu J H 2011 *Dalton Trans.* **40** 7967
[36] Kumar S, Pickett M D, Strachan J P, Gibson G, Nishi Y and Williams R S 2014 *Adv. Mater.* **26** 7505
[37] Shi Q W, Huang W X, Lu T C, Zhang Y X, Yue F, Qiao S and Xiao Y 2014 *Appl. Phys. Lett.* **104** 071903
[38] Quackenbush N F *et al* 2013 *Nano Lett.* **13** 4857
[39] Chen C H and Fan Z Y 2009 *Appl. Phys. Lett.* **95** 262106
[40] Rathi S, Lee I Y, Park J H, Kim B J, Kim H T and Kim G H 2014 *ACS Appl. Mater. Interfaces* **6** 19718
[41] Yang Z and Ramanathan S 2011 *Appl. Phys. Lett.* **98** 192113
[42] Biermann S, Poteryaev A, Lichtenstein A I and Georges A 2005 *Phys. Rev. Lett.* **94** 026404
[43] Kim H T, Lee Y W, Kim B J, Chae B G, Yun S J, Kang K Y, Han K J, Yee K J and Lim Y S 2006 *Phys. Rev. Lett.* **97** 266401
[44] Marini C *et al* 2008 *Phys. Rev.* B **77** 235111
[45] Schilbe P 2002 *Physica* B **316** 600
[46] Baik J M, Kim M H, Larson C, Wodtke A M and Moskovits M 2008 *J. Phys. Chem.* C **112** 13328
[47] Jones J A C, Berweger S, Wei J, Cobden D and Raschke M B 2010 *Nano Lett.* **10** 1574
[48] Zhang S, Chou J Y and Lauhon L J 2009 *Nano Lett.* **9** 4527
[49] Arcangeletti E, Baldassarre L, Castro D D, Lupi S, Malavasi L, Marini C, Perucchi A and Postorino P 2007 *Phys. Rev. Lett.* **98** 196406
[50] Okazaki K, Sugai S, Muraoka Y and Hiroi Z 2006 *Phys. Rev.* B **73** 165116
[51] Li W W, Yu Q, Liang J R, Jiang K, Hu Z G, Liu J, Chen H D and Chu J H 2011 *Appl. Phys. Lett.* **99** 241903
[52] Wall S, Wegkamp D, Foglia L, Appavoo K, Nag J, Haglund R F, Stahler J and Wolf M 2012 *Nat. Commun.* **3** 721
[53] Zimmers A, Aigouy L, Mortier M, Sharoni A, Wang S, West K G, Ramirez J G and Schuller I K 2013 *Phys. Rev. Lett.* **110** 056601
[54] Ruzmetov D, Senanayake S D, Narayanamurti V and Ramanathan S 2008 *Phys. Rev.* B **77** 195442
[55] Koethe T C *et al* 2006 *Phys. Rev. Lett.* **97** 116402
[56] Anibal G and Clarence C Y K 1972 *Phys. Rev.* B **5** 3138
[57] Li W W, Zhu J J, Xu X F, Jiang K, Hu Z G, Zhu M and Chu J H 2011 *J. Appl. Phys.* **110** 013504
[58] Hu S L, Li S Y, Ahuja R, Granqvist C G, Hermansson K, Niklasson G A and Scheicher R H 2013 *Appl. Phys. Lett.* **103** 161907